

Robust Time-Varying Parameter Identification for Composite Load Modeling

Chong Wang¹, Member, IEEE, Zhaoyu Wang², Member, IEEE, Jianhui Wang³, Senior Member, IEEE, and Dongbo Zhao, Senior Member, IEEE

Abstract—With the increasing integration of uncertain resources, e.g., renewables, electric vehicles, and demand responses, it is imperative to understand the characteristics of loads for power system analysis and control. Challenges of load modeling come from a variety of load components and time-varying compositions. In addition, the existence of outliers in measurements further complicates the problem. This paper proposes a robust time-varying parameter identification technique for composite ZIP and induction motor load models. A batch-model regression form, including time-varying parameters, is established based on state transition models and observation models with current observations and previous predictions to guarantee data redundancy. To deal with outliers, down-weighting coefficients of measurements are calculated with a projection statistics approach. Based on the batch-model regression and the down-weighting coefficients, parameter identification at each sample time is formulated as a weighted least squares optimization, which is solved by the Newton-Raphson approach with the previous estimated parameters as the initial iteration values. In addition, parameters' sensitivities to different outliers in measurements are analyzed. Results on the IEEE 57-bus system and IEEE 118-bus system show that the proposed algorithm can robustly identify time-varying parameters for the composite load models.

Index Terms—Composite load model, outliers, parameter identification, robust, time-varying.

NOMENCLATURE

Parameters/States of Composite Load Model

t	Index of sample time.
$a_{p,t}, b_{p,t}, c_{p,t}$	Parameters for active power of ZIP load at t .
$a_{q,t}, b_{q,t}, c_{q,t}$	Parameters for reactive power of ZIP load at t .
H_t	Inertia constant of induction motor at t .
$i_{d,t}$	d -axis stator current at t .

$i_{q,t}$	q -axis stator current at t .
$P_{ZIP,0}$	Base active power consumption of ZIP load.
$P_{ZIP,t}$	Active power consumption of ZIP load at t .
$P_{IM,t}$	Active power consumption of induction motor at t .
$P_{CL,t}$	Active power consumption of composite load at t .
$Q_{ZIP,0}$	Base reactive power consumption of ZIP load.
$Q_{ZIP,t}$	Reactive power consumption of ZIP load at t .
$Q_{IM,t}$	Reactive power consumption of induction motor at t .
$Q_{CL,t}$	Reactive power consumption of composite load at t .
$R_{r,t}$	Rotor resistance at t .
$R_{s,t}$	Stator resistance at t .
s_t	Rotor slip at t .
T_{m0}	Initial load torque.
$U_{d,t}$	d -axis bus voltage at t .
$U_{q,t}$	q -axis bus voltage at t .
V_0	Nominal voltage magnitude.
V_t	Voltage magnitude of the bus of interest at t .
$v'_{d,t}$	d -axis transient voltage at t .
$v'_{q,t}$	q -axis transient voltage at t .
$X_{m,t}$	Magnetizing reactance at t .
$X_{r,t}$	Rotor reactance at t .
$X_{s,t}$	Stator reactance at t .
X_t	Short circuit reactance at t .
$\lambda_{p,t}, \lambda_{q,t}$	Proportions of ZIP load in active and reactive power of composite load, respectively.

Notation for Algorithm

τ_t	Vector of bus voltage at t .
ζ_t	Vector of IM states at t .
ξ_t	Vector of time-varying parameters t .
$\omega_{\xi,t}, \omega_{x,t}$	Vectors of process noises at t .
v_t	Vector of measurement noises at t .
\mathbf{f}	Nonlinear function vector of state transition equations.
\mathbf{h}	Nonlinear function vector of observation equations.
\mathbf{R}_t	Diagonal covariance matrix with respect to the batch model.
\mathbf{x}_t	Vector of states and parameters at t .
$\tilde{\mathbf{x}}_{t t-1}$	Prediction at t based on estimation at $t-1$.
$\tilde{\mathbf{x}}_{t-1}, \tilde{\tau}_{t-1}$	Estimations at $t-1$.

Manuscript received March 30, 2017; revised July 1, 2017 and August 21, 2017; accepted September 20, 2017. Date of publication September 26, 2017; date of current version December 19, 2018. This work was supported by the U.S. Department of Energy Office of Electricity Delivery and Energy Reliability. Paper no. TSG-00441-2017. (Corresponding author: Zhaoyu Wang.)

C. Wang and Z. Wang are with the Department of Electrical and Computer Engineering, Iowa State University, Ames, IA 50011 USA (e-mail: wangc@iastate.edu; wzy@iastate.edu).

J. Wang is with the Department of Electrical Engineering, Southern Methodist University, Dallas, TX 75275 USA, and also with the Energy Systems Division, Argonne National Laboratory, Argonne, IL 60439 USA (e-mail: jianhui.wang@ieec.org).

D. Zhao is with Energy Systems Division, Argonne National Laboratory, Argonne, IL 60439 USA (e-mail: dongbo.zhao@anl.gov).

Color versions of one or more of the figures in this paper are available online at <http://ieeexplore.ieee.org>.

Digital Object Identifier 10.1109/TSG.2017.2756898

\mathbf{X}_t	Input vector of batch-mode regression at t .
$\mathbf{X}_t^{(n)}, \mathbf{X}_t^{(n+1)}$	Vectors at n and $n+1$ iterations, respectively.
$\tilde{\mathbf{X}}_t$	Estimation of batch-mode regression at t .
\mathbf{y}_t	Output vector of batch-mode regression at t .
G, J, F, H	Nonlinear function vectors.
\mathbf{e}_t	Batch-model noise vector at t .
\mathbf{M}_t	k -dimensional matrix.
$\mathbf{d}_{j,t}$	j th row vector in \mathbf{M}_t .
μ, σ	Mean and standard deviation.
$MD_{j,t}$	Mahalanobis distance of $\mathbf{d}_{j,t}$ at t .
$PS_{j,t}$	Projection statistics value of $\mathbf{d}_{j,t}$ at t .
$\omega_{j,t}$	Weighted coefficient of measurement j at t .
D	A constant.
$v_{T,t}$	True value at t .
$v_{E,t}$	Estimated value at t .
RE_t	Relative error at t .
MVP	Mean value of parameter.
MAPE	Mean absolute percentage error.

I. INTRODUCTION

THE INTEGRATION of uncertain power resources [1]–[3] and loads results in high-frequency changes of load characteristics, which have great influences on power system operation [4]–[6]. In addition, the outliers in measurements [7] could compromise model identification results. Therefore, it is imperative to develop new algorithms that are robust to bad measurements and have the ability to tract time-varying load characteristics.

There are two main approaches, i.e., the component-based approach and the measurement-based approach, for load modeling [8]. Some research focused on the component-based model [9], [10]. This model has a good physical representation of terminal devices, and it can be used in different operation conditions. However, since physical behaviors and their mathematical relations cannot be always achieved, it is often difficult to apply this model to complex loads. For the measurement-based approach [11]–[15], the measurements at buses of interest are used to derive the load pattern. The measurement-based model is a generic representation without knowing the detailed characteristics of loads, and it is based on practical measurements from systems. However, a model derived from measurements at a specific location during a certain period lacks of generalizability. To use the measurement-based approach, the load structure should be first determined. The common load structures include three categories: static model, dynamic model, and composite model.

- *Static model*: This model represents active and reactive power as functions of voltage/frequency but not time. Common static models consist of ZIP models [16], exponential models [17] and frequency dependent models [18]. The static models in the Electric Power Research Institute (EPRI) LOADSYN program include the three common static models [19], [20].
- *Dynamic model*: It expresses active and reactive power as functions of not only voltage but time. One typical dynamic load model is a third-order induction motor

(IM) model [16]. Another dynamic model is the exponential recovery load (ERL) model, which is often applied to the scenario that loads slowly recover within a time period [21], [22]. This model can also be employed to express on-load tap changers (OLTCs) that recover the nominal voltage after disturbances.

- *Composite model*: Based on the static and dynamic models, many research studies focus on composite load models [23], [24], which can offer more accurate characteristics. For example, composite loads, including ZIP models and IM models, are most widely used for dynamic analysis in the U.S. industry [25]. Complex load (CLOD) models [26], including large/small motors, constant MVA, shunt capacitors and transformer saturation effects, are developed in the PSS@E software to represent dynamic load behaviors. In addition, a composite load model with 80% static load and 20% dynamic load is implemented by the Western Systems Coordinating Council (WSCC). For this model, the static part is derived based on the existing data provided by WSCC members, and the dynamic part is represented by an induction motor model. To improve the model, WECC added the electrical distance between the end-users and the transmission system. By 2012, the WECC load model has been tested and implemented in software such as Siemens PTI PSS@E and PowerWorld Simulator.

Parameters of the selected model structure are optimized to ensure a minimum error between the recorded data and the model output. Many algorithms based on statistical techniques and heuristic techniques are proposed to optimize load model parameters. With respect to statistical techniques, weighted least square-based estimation [27], least square-based parameter estimation [28], maximum likelihood-based estimation [29] and gradient-based parameter estimation [30] have been proposed to identify the parameters. For the weighted least square approach, it can be used to solve the problem with unequal variances of noises, and the weight of each measurement depends on its variability. High variability effects of measurements can be reduced. However, it is not easy to determine the weights, and the weights may increase the computational complexity. For the maximum likelihood approach, the probability density function of measurements is needed to define the likelihood function, which may be unknown in practice. In addition, this approach is a time-consuming task. The gradient-based approach is vulnerable to data pollution. With respect to heuristic techniques, genetic algorithm [31], neural network [32] and simulated annealing algorithm [33] have been proposed to identify the parameters. The genetic algorithm is a multi-point search algorithm that can be easily adjusted to different problems. However, the high computational cost is a main obstacle in applying the genetic algorithm to complex models. The neural network approach can adaptively train and update models based on measurements without knowing the structure of load models. However, it is difficult to determine algorithm settings, and it has a slow convergence rate. The simulated annealing algorithm does not require mathematical representations of load models, and can handle highly nonlinear models. However,

repeated annealing with a schedule is very slow, especially when the cost function is difficult to compute. In addition, there are some other approaches based on the local model network (LMN) [34] and historical load data [35] for load modeling. In [34], the proposed LMN-based method requires no pre-defined standard load models, and can achieve maximum the generalizability with the best linear or nonlinear structure by using the hierarchical binary tree learning algorithm. Borojeni *et al.* [35] presents a generic approach for modeling historical load data, and the proposed approach can deal with non-seasonal and seasonal cycles of load data with moving-average and auto-regressive components, which only rely on historical load data without requiring any additional inputs.

The integration of uncertain resources results in high frequency of changes of load model parameters, i.e., time-varying parameters. In addition, outliers in measurements may compromise estimated results for these parameters. To deal with these challenges, a robust time-varying parameter identification technique for the static ZIP load model is proposed in [36]. However, dynamic characteristics of loads are not included in [36]. The contribution of this paper is to propose a robust time-varying parameter identification technique for static and dynamic loads considering possible outliers in measurements. To ensure data redundancy, current observations and previous predictions are used to construct a batch-mode regression form based on the state transition models and the observation models. To reduce the negative impacts of outliers, a projection statistics (PS) approach is used to calculate the robust distances of a k -time sequence to obtain the down-weighting coefficient for each measurement. Robust time-varying parameter identification at each sample time is formulated as an optimization problem with minimizing the weighted squares error, and the Newton-Raphson approach is used to solve the optimization problem.

The rest of the paper is organized as follows. Section II describes the framework of the proposed robust time-varying parameter identification. Section III presents the time-varying ZIP and IM load models, and Section IV shows the robust time-varying parameter identification. Section V presents simulation results and Section VI concludes the paper.

II. FRAMEWORK OF ROBUST TIME-VARYING PARAMETER IDENTIFICATION

This section shows the framework of the robust time-varying parameter identification. First, the time resolution of the model and the definitions of some blocks in the framework are introduced, and then the relations between the blocks are presented.

A. Time Resolution and Definitions of Blocks

Fig. 1 shows the typical time frame for a full range of power system phenomena from microseconds to hours [37]. The dynamics of loads investigated in this paper belong to the topic of electromechanical transient, and the range of the time resolution is from 10^{-2} s to 1s. The dynamic load model

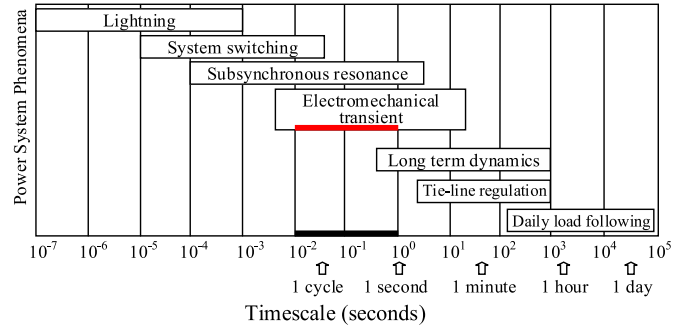


Fig. 1. Range of power system phenomena from microseconds to hours.

investigated in this paper can be deployed in power system dynamic studies.

To implement robust parameter identification at each sample time, several critical blocks are included, as shown in Fig. 2. The robustness means that the proposed method has high identification accuracy for time-varying parameters of load models even when there are outliers in measurements.

1) *State Transition Model*: Given that states/parameters are time-varying and they have relations at adjacent sample time, the state transition model relates these time-varying states/parameters. The state transition model includes a series of discrete differential equations. Its inputs consist of estimated parameters/states at the preceding sample time, and the outputs are discrete differential equations.

2) *Observation Model*: The observation model represents the mathematical relation between states/parameters and practical measurements, and it includes a group of algebraic equations. Its inputs consist of estimated parameters/states at the preceding sample time and the measurements at the current sample time. Its outputs are a group of algebraic equations representing the relation between states/parameters and measurements.

3) *Projection Statistics*: The PS approach is used to achieve the weighted coefficient for each measurement. Outliers will have small weighted coefficients. The inputs of this block consist of the estimated states/parameters at the preceding sample time and the measurements at the current sample time. The outputs are weighted coefficients for measurements.

4) *Batch Model*: The batch model includes a group of regression equations derived from the state transition model and the observation model, including states/parameters and measurements. Its inputs include the state transition model and the observation model, and its outputs consist of the regression models.

5) *Weighted Least Squares*: At each sample time, parameter identification is formulated as a weighted least squares optimization. Its inputs include the batch model, wighted coefficients, and the initial iteration values. Its outputs are the estimated parameters/states.

B. Relations of Blocks

The relations between different blocks are shown in Fig. 2. For example, at the sample time t , the state transition model is established based on the estimated parameters and states at the

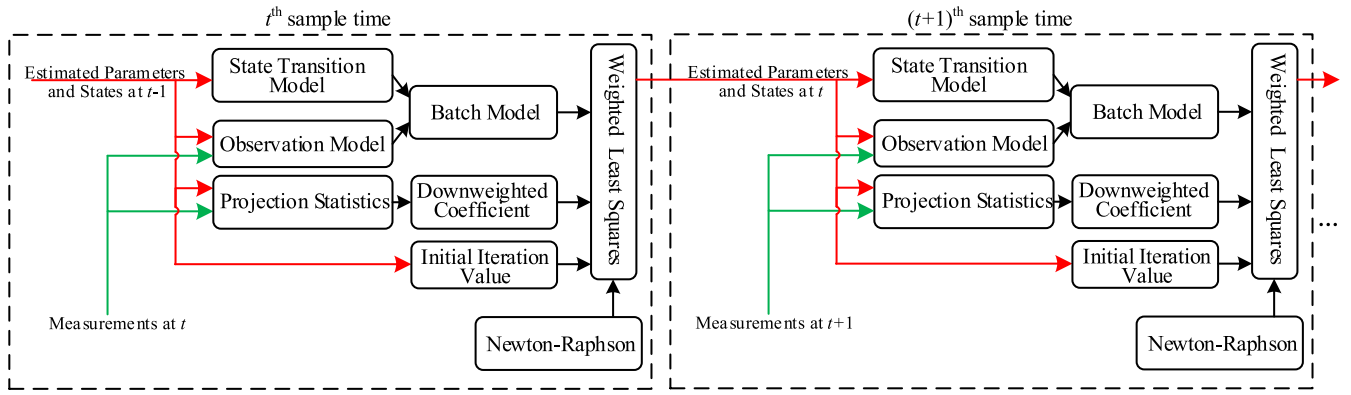


Fig. 2. Framework of robust time-varying parameter identification.

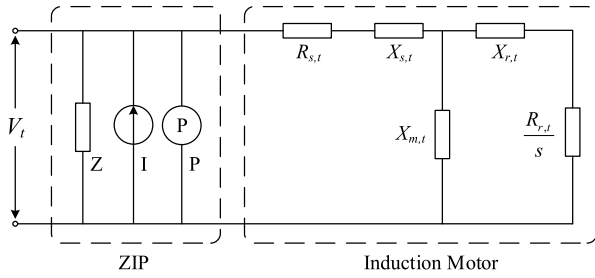


Fig. 3. Equivalent circuit of ZIP and IM load model.

sample time $t - 1$. The observation model is achieved based on the estimated parameters and states at the sample time $t - 1$ and the measurements at the sample time t . The batch-mode regression, in which current measurements and previous estimations guarantee data redundancy, is constructed by using the established state transition model and the observation model. To deal with possible outliers, down-weighting coefficients for measurements are achieved by calculating robust distances of a k -time sequence with the PS approach. To estimate states and parameters, a nonlinear model of the least square with down-weighting coefficients is established. The Newton-Raphson approach, with the estimated parameters and states at the sample time $t - 1$ as the initial iteration values, is employed to solve the nonlinear model.

III. TIME-VARYING LOAD MODELING

This section first shows the load model with time-varying parameters, including a ZIP model and a IM model. Then, a batch model is established based on the time-varying ZIP and IM models. Fig. 3 shows the equivalent circuit of the composite ZIP and IM model. The mathematical models are introduced in the following subsections.

A. Time-Varying ZIP Model

The ZIP model is one of typical static load models. It consists of constant impedance (Z), constant current (I) and constant power (P) components. Considering different weather conditions, customer behaviors and system operation conditions, the percentages of Z, I and P are usually time-varying.

Its mathematical formulations can be expressed as follows.

$$P_{ZIP,t} = P_{ZIP,0} \left(a_{p,t} \left(\frac{V_t}{V_0} \right)^2 + b_{p,t} \left(\frac{V_t}{V_0} \right) + c_{p,t} \right) \quad (1)$$

$$Q_{ZIP,t} = Q_{ZIP,0} \left(a_{q,t} \left(\frac{V_t}{V_0} \right)^2 + b_{q,t} \left(\frac{V_t}{V_0} \right) + c_{q,t} \right) \quad (2)$$

where $a_{p,t}$, $b_{p,t}$ and $c_{p,t}$ satisfy $a_{p,t} + b_{p,t} + c_{p,t} = 1 \quad \forall t$, and $a_{q,t}$, $b_{q,t}$ and $c_{q,t}$ satisfy $a_{q,t} + b_{q,t} + c_{q,t} = 1 \quad \forall t$.

B. Time-Varying IM Model

The structure of the IM model is shown in Fig. 3. To include the impacts of different weather conditions, customer behaviors and so on, the parameters of the IM model are considered to be time-varying. The IM model can be expressed as:

$$\frac{dv'_{d,t}}{dt} = \frac{-R_{r,t}}{X_{r,t} + X_{m,t}} \left(v'_{d,t} + \frac{X_{m,t}^2}{X_{r,t} + X_{m,t}} i_{q,t} \right) + s_t v'_{q,t} \quad (3)$$

$$\frac{dv'_{q,t}}{dt} = \frac{-R_{r,t}}{X_{r,t} + X_{m,t}} \left(v'_{q,t} - \frac{X_{m,t}^2}{X_{r,t} + X_{m,t}} i_{d,t} \right) - s_t v'_{d,t} \quad (4)$$

$$\frac{ds_t}{dt} = \frac{1}{2H_t} \left(T_{m0}(1 - s_t)^2 - v'_{d,t} i_{d,t} - v'_{q,t} i_{q,t} \right) \quad (5)$$

where the d -axis stator current $i_{d,t}$ and the q -axis stator current $i_{q,t}$ are calculated as follows.

$$i_{d,t} = \frac{R_{s,t}(U_{d,t} - v'_{d,t}) + X'_t(U_{q,t} - v'_{q,t})}{R_{s,t}^2 + X'_t{}^2} \quad (6)$$

$$i_{q,t} = \frac{R_{s,t}(U_{q,t} - v'_{q,t}) - X'_t(U_{d,t} - v'_{d,t})}{R_{s,t}^2 + X'_t{}^2} \quad (7)$$

where the d -axis bus voltage $U_{d,t}$ and the q -axis bus voltage $U_{q,t}$ satisfy the following equation.

$$V_t = \sqrt{U_{d,t}^2 + U_{q,t}^2} \quad (8)$$

The short circuit reactance X'_t is expressed as

$$X'_t = X_{s,t} + \frac{X_{m,t} \cdot X_{r,t}}{X_{m,t} + X_{r,t}} \quad (9)$$

With the states, time-varying parameters and the bus voltage, the active and reactive power of the IM model can be expressed as

$$P_{IM,t} = \left[R_{s,t} \left(U_{d,t}^2 + U_{q,t}^2 - U_{d,t}v'_{d,t} - U_{q,t}v'_{q,t} \right) - X'_t \left(U_{d,t}v'_{q,t} - U_{q,t}v'_{d,t} \right) \right] / (R_{s,t}^2 + X_t'^2) \quad (10)$$

$$Q_{IM,t} = \left[X'_t \left(U_{d,t}^2 + U_{q,t}^2 - U_{d,t}v'_{d,t} - U_{q,t}v'_{q,t} \right) - R_{s,t} \left(U_{d,t}v'_{q,t} - U_{q,t}v'_{d,t} \right) \right] / (R_{s,t}^2 + X_t'^2). \quad (11)$$

C. Time-Varying Composite Model

With active and reactive power of the composite ZIP and IM model, the total active and reactive power can be computed as

$$P_{CL,t} = \lambda_{p,t} P_{ZIP,t} + (1 - \lambda_{p,t}) P_{IM,t} \quad (12)$$

$$Q_{CL,t} = \lambda_{q,t} Q_{ZIP,t} + (1 - \lambda_{q,t}) Q_{IM,t} \quad (13)$$

Since the ZIP model represents active/reactive power as functions of voltage and the IM model relates active/reactive power as functions of voltage/time, the impact of system frequency is not involved.

For the models (1)-(13), there are bus voltage variables, IM state variables, and time-varying parameter variables, which are denoted as

$$\tau_t = [U_{d,t}, U_{q,t}]^T \quad (14)$$

$$\zeta_t = [v'_{d,t}, v'_{q,t}, s_t]^T \quad (15)$$

$$\xi_t = [R_{s,t}, X_{s,t}, X_{m,t}, X_{r,t}, R_{r,t}, H_t, a_{p,t}, b_{p,t}, a_{q,t}, b_{q,t}, \lambda_{p,t}, \lambda_{q,t}]^T \quad (16)$$

Normally, parameter changes are very small within a short period, and the transition of parameters between different time intervals can be expressed as

$$\xi_t = \xi_{t-1} + \omega_{\xi,t} \quad (17)$$

where $\omega_{\xi,t}$ is the process noise vector.

Based on (3)-(5) and (17), discrete state transitions and parameter transitions can be generalized as

$$\mathbf{x}_t = \mathbf{f}(\mathbf{x}_{t-1}, \tau_{t-1}) + \omega_{x,t} \quad (18)$$

where \mathbf{x}_t is a vector, which defined as $[\zeta_t^T, \xi_t^T]^T$, and $\omega_{x,t}$ is the process noise vector.

With (1), (2), and (9)-(13), an observation equation is generalized as

$$\mathbf{z}_t = \mathbf{h}(\mathbf{x}_t, \tau_t) + v_{h,t} \quad (19)$$

where \mathbf{z}_t is the measurement vector which includes active power, reactive power and bus voltage, \mathbf{h} is the nonlinear function vector, and $v_{h,t}$ is the measurement noise vector.

D. Batch-Model Construction

This section shows the batch-mode construction. With the estimation vectors $\tilde{\mathbf{x}}_{t-1}$ and $\tilde{\tau}_{t-1}$, the prediction $\tilde{\mathbf{x}}_{t|t-1}$ at time t can be achieved as follows.

$$\tilde{\mathbf{x}}_{t|t-1} = \mathbf{f}(\tilde{\mathbf{x}}_{t-1}, \tilde{\tau}_{t-1}) \quad (20)$$

Integrate (19) and (20) to one matrix form, and we can get

$$\begin{bmatrix} \tilde{\mathbf{x}}_{t|t-1} \\ \mathbf{z}_t \end{bmatrix} = \begin{bmatrix} \mathbf{x}_t \\ \mathbf{h}(\mathbf{x}_t, \tau_t) \end{bmatrix} + \begin{bmatrix} \omega_{x,t} \\ v_{h,t} \end{bmatrix} \quad (21)$$

which can be generalized as

$$\mathbf{y}_t = \mathbf{g}(\mathbf{X}_t) + \mathbf{e}_t \quad (22)$$

where $\mathbf{X}_t = [\mathbf{x}_t^T \tau_t^T]^T$ include parameter variables, IM state variables and bus voltage variables. \mathbf{y}_t can be expressed as $[\tilde{\mathbf{x}}_{t|t-1}^T \mathbf{z}_t^T]^T$, and $\mathbf{e}_t = [\omega_{x,t}^T v_{h,t}^T]^T$ is the batch-model noise vector, which satisfies $E[\mathbf{e}_t \mathbf{e}_t^T] = \mathbf{R}_t$.

IV. ROBUST TIME-VARYING PARAMETER IDENTIFICATION

This section first shows a typical optimization model for parameter/state estimation. Second, down-weighting coefficients for measurements are achieved by calculating the distances of a k -time sequence with the PS approach. Third, the optimization model with down-weighting coefficients of measurements is presented, and the solution algorithm based on the Newton-Raphson method is employed.

A. Parameter Identification Model

Since \mathbf{y}_t in (22) has some noises, the objective is to find \mathbf{X}_t , which ensures that the error between the estimation outputs and the measurements is minimum.

$$\tilde{\mathbf{X}}_t = \arg \min_{\mathbf{X}_t} G(\mathbf{X}_t)$$

$$G(\mathbf{X}_t) = (\mathbf{y}_t - \mathbf{g}(\mathbf{X}_t))^T \cdot \mathbf{R}_t \cdot (\mathbf{y}_t - \mathbf{g}(\mathbf{X}_t)) \quad (23)$$

where (23) is a nonlinear optimization problem. Minimizing this optimization can achieve the estimated parameters and states. However, this model includes all recorded measurements, which may consist of outliers, resulting in the corruption of the estimated results. Hence, the next subsection introduces an approach to deal with possible outliers.

B. Down-Weighting Approach Based on Projection Statistics

The critical point of the down-weighting approach is to systematically down-weight the proportion of possible outliers, rather than removing them directly. This approach can not only keep an acceptable level of statistical efficiency, but have a good robustness, typically for some boundary outliers that are beyond but close to the outlier detection threshold. A projection statistic value is a distance of a data point from the bulk of the point cloud. To detect outliers in measurements, we first establish a k -dimensional matrix \mathbf{M} , which consists of residuals and predictions.

$$\mathbf{M}_t = [\mathbf{m}_{t-k+1}, \mathbf{m}_{t-k+2}, \dots, \mathbf{m}_t] \quad (24)$$

$$\mathbf{m}_{t-k+1} = \begin{bmatrix} \tilde{\mathbf{X}}_{t-k+1|t-k} \\ \mathbf{y}_{t-k+1} - \mathbf{g}(\tilde{\mathbf{X}}_{t-k+1|t-k}) \end{bmatrix} \quad (25)$$

where $\tilde{\mathbf{X}}_{t-k+1|t-k}$ is the predictions at time $t-k+1$ with the estimation at $t-k$.

The distance of a point from the cloud can be used to identify outliers. One distance proposed by Donoho [38] is the Mahalanobis distance that is expressed as

$$MD_{j,t} = \max_{\|\mathbf{u}=1\|} \frac{\mathbf{d}_{j,t}^T \mathbf{u} - \mu}{\sigma} \quad (26)$$

where μ and σ are the sample mean and standard deviation of the projections of $\mathbf{d}_{j,t}$ on all directions of the vector \mathbf{u} . However, this distance should include all directions, and is computationally intractable. To reduce computational burden, the sample median absolute deviation and the sample median were suggested by Donoho and Gasko [39] to calculate the distance, as shown in (27). This distance is defined as the projection statistics value, which is expressed as

$$PS_{j,t} = \max_{\|\mathbf{u}=1\|} \frac{\left| \mathbf{d}_{j,t}^T \mathbf{u} - \text{med}_i \left(\mathbf{d}_{i,t}^T \mathbf{u} \right) \right|}{1.4826 \text{med}_j \left| \mathbf{d}_{j,t}^T \mathbf{u} - \text{med}_i \left(\mathbf{d}_{i,t}^T \mathbf{u} \right) \right|} \quad (27)$$

where $\text{med}(\ast)$ denotes the median of the vector \ast . In practice, it is difficult to get the projections on each direction, and it was suggested in [39] that only vectors \mathbf{u} that originate at median and pass through $\mathbf{d}_{j,t}$ are investigated.

With (27), the distance of each point, i.e., the row of the matrix \mathbf{M} , from the data can be calculated. When it is larger than a given threshold, the corresponding point can be considered as an outlier, which is downweighted by the following formulation.

$$w_{j,t} = \min \left(1, \frac{D^2}{PS_{j,t}^2} \right) \quad (28)$$

where D is selected to be 1.5 that can have statistical efficiency [40].

C. Down-Weighting Parameter Identification Model

With the down-weighting coefficients, the parameter identification model can be rewritten as

$$\begin{aligned} \tilde{\mathbf{X}}_t &= \arg \min_{\mathbf{X}_t} J(\mathbf{X}_t) \\ J(\mathbf{X}_t) &= (\mathbf{y}_t - \mathbf{g}(\mathbf{X}_t))^T \cdot \mathbf{W}_t \cdot \mathbf{R}_t \cdot (\mathbf{y}_t - \mathbf{g}(\mathbf{X}_t)) \end{aligned} \quad (29)$$

where \mathbf{W}_t is a diagonal matrix defined as $\text{diag}[w_{1,t}, w_{2,t}, \dots]$. This model is a nonlinear optimization model, and the estimations at time t should satisfy the following condition.

$$\mathbf{F}(\mathbf{X}_t) = \frac{\partial J(\mathbf{X}_t)}{\partial \mathbf{X}_t} = \mathbf{0} \quad (30)$$

where \mathbf{F} is a nonlinear function vector. In this paper, it is assumed that the parameters are time-varying but not mutant. Thus, for the estimation at time t , we take the estimated $\tilde{\mathbf{X}}_{t-1}$ at time $t-1$ as an initial iteration value, and use the Newton-Raphson method to solve the nonlinear equation (30).

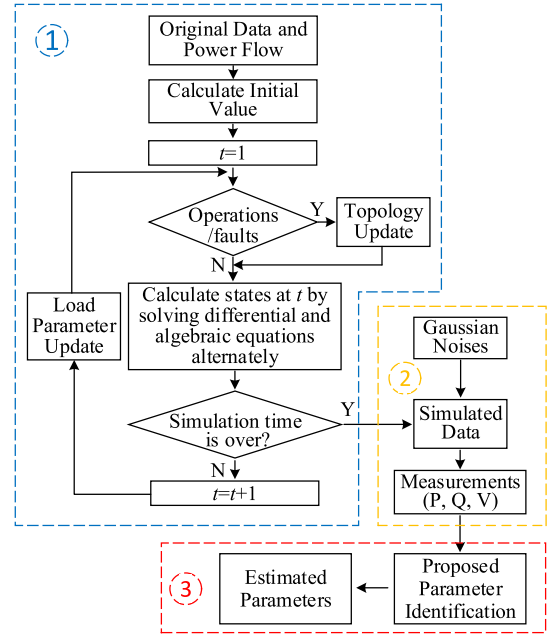


Fig. 4. Simulation processes.

D. Sensitivity of Parameters to Outliers

Outliers in measurements, i.e., active power, reactive power and voltage, can corrupt the estimations, and their impacts on different estimations may be different. This section shows the analysis of sensitivity of parameters to outliers. According to the Newton-Raphson method, the estimations are updated with the following equation.

$$\mathbf{X}_t^{(n+1)} = \mathbf{X}_t^{(n)} - \left[\mathbf{H}(\mathbf{X}_t^{(n)}) \right]^{-1} \cdot \mathbf{F}(\mathbf{X}_t^{(n)}) \quad (31)$$

where \mathbf{H} is the Hessian matrix, which is expressed as

$$\mathbf{H}(\mathbf{X}_t^{(n)}) = \frac{\partial \mathbf{F}}{\partial \mathbf{X}} \Big|_{\mathbf{X}_t^{(n)}} \quad (32)$$

The updating equation shows that the amount of estimation update depends on the values of the function \mathbf{F} and the inverse Hessian matrix. For the inverse Hessian matrix, we can use its eigenvalue to qualitatively analyze the amount of estimation update. For example, if the i^{th} eigenvalue of the inverse Hessian matrix and the i^{th} element of the vector \mathbf{F} are both large, the amount of the i^{th} parameter update in the vector \mathbf{X}_t will be accordingly large.

V. CASE STUDIES

This section validates the proposed robust time-varying parameter identification. First, the effectiveness of the proposed method is verified by the case studies. Second, sensitivities of different parameters to outliers in the measurements of active power, reactive power and voltage are analyzed. The IEEE 57-bus system and the IEEE 118-bus system with composite ZIP and IM loads are used to validate the proposed method. To illustrate the results, we only focus on the measurements of the buses of interest.

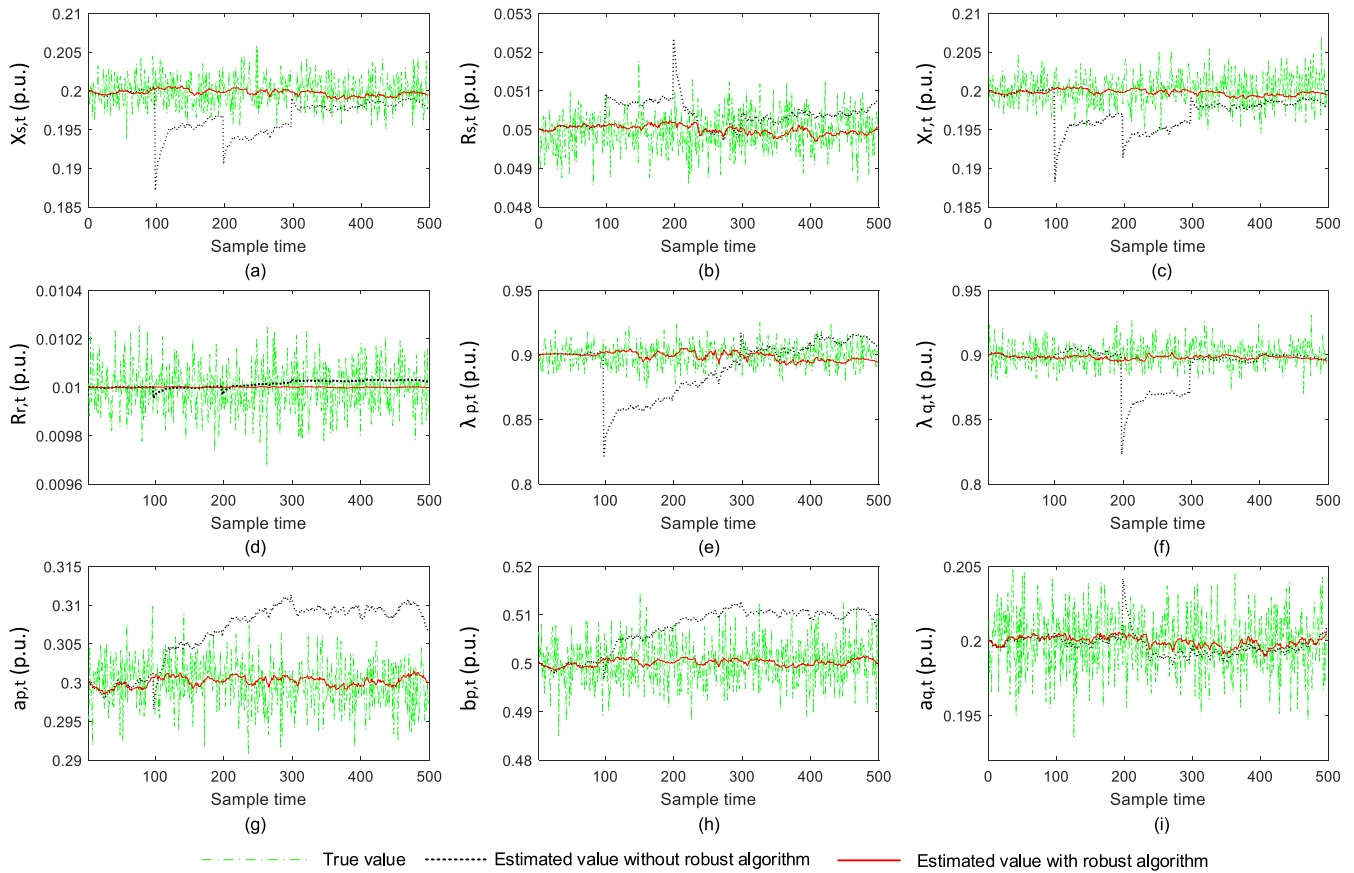


Fig. 5. Parameter identification results comparison for $X_{s,t}$ (a), $R_{s,t}$ (b), $X_{r,t}$ (c), $R_{r,t}$ (d), $\lambda_{p,t}$ (e), $\lambda_{q,t}$ (f), $a_{p,t}$ (g), $b_{p,t}$ (h), and $a_{q,t}$ (i).

A. Simulation Processes

Fig. 4 shows the simulation processes, and the algorithm 1 shows the pseudocodes for the simulation processes. There are three main steps.

1) *First Step:* Time-domain simulations (TDS) are performed in this step to obtain the simulated data, e.g., active/reactive power and voltage. The original data of the system and the power flow are used to calculate the initial state value. At a certain point, there are operations/faults in the system, and the system topology is updated correspondingly. With the preceding states and the updated topology, the states at the current sample time are calculated by solving differential-algebraic equations (DAEs) alternately. If the simulation time is over, simulated data are obtained. If not, update load parameters and achieve the states for the following samples repeatedly.

2) *Second Step:* The second step is to generate measurements (GMT) of voltage, active power, and reactive power. Based on the simulated data from the first step, Gaussian noises are added to these data, and get the simulated measurements.

3) *Third Step:* The third step is to use the proposed time-varying parameter identification (TVPI) technique to estimate the parameters at each sample time based on the simulated measurements obtained from the second step.

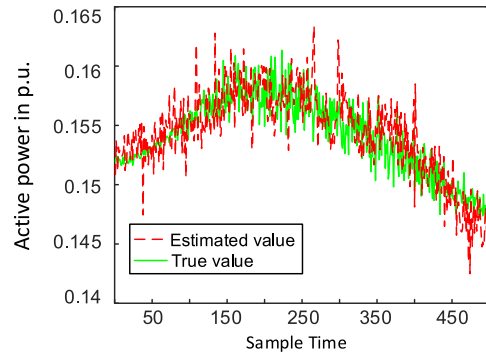


Fig. 6. Estimated active power and true active power.

B. 57-Bus System

1) *Effectiveness of Proposed Method:* This section shows the effectiveness of the proposed method. The mean values of the parameters $R_{s,t}$, $X_{s,t}$, $X_{m,t}$, $X_{r,t}$, $R_{r,t}$, H_t , $a_{p,t}$, $b_{p,t}$, $a_{q,t}$, $b_{q,t}$, $\lambda_{p,t}$, $\lambda_{q,t}$ for the composite ZIP and IM model are 0.05, 0.2, 4, 0.2, 0.01, 20, 0.3, 0.5, 0.2, 0.4, 0.9 and 0.9. For each parameter, a Gaussian random variable with zero mean and standard deviation MVP/100 is added to simulate continuous parameter changes. MVP is the mean value of the parameter. Each measurement is assumed to be corrupted with a Gaussian noise with zero mean and standard deviation 0.005. There are

Algorithm 1 Pseudocodes for Simulation Processes

```

1: function TDS(Original Data)
2:   Power flow calculation
3:   Initial value calculation
4:   for  $t = 1 \rightarrow T$  do
5:     while Operations/faults occur do
6:       Topology update
7:     end while
8:     Obtain simulated data at  $t$  with DAEs
9:   end for
10: end function
11:
12: function GMT(Simulated Data)
13:   for  $t = 1 \rightarrow T$  do
14:     Measurement[t]  $\leftarrow$  SimulatedData[t] + Noise[t]
15:   end for
16: end function
17:
18: function TVPI(Measurements)
19:   for  $t = 1 \rightarrow T$  do
20:     With (1)-(19), construct batch model (20)-(22).
21:     Calculate downweighted coefficient  $w_{j,t}$  with (24)-(28).
22:     Construct identification model (29).
23:     while Tolerance > Given Value do
24:       Update estimated values with (31) and (32).
25:     end while
26:   end for
27: end function

```

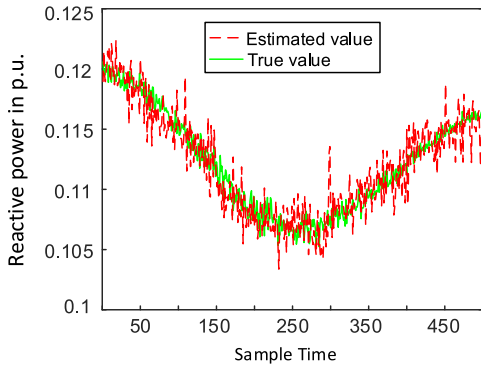


Fig. 7. Estimated reactive power and true reactive power.

500 samples and the sample time is 0.1s. We assume that the measurements of active power, reactive power, the real part of voltage, and the imaginary part of voltage have outliers with 40% at the sample time 100, 200, 300, and 400, respectively. We use the metrics of *relative error* (RE) and *mean absolute percentage error* (MAPE) to evaluate the accuracy of the proposed time-varying parameter identification technique.

Fig. 5 shows the parameter identification results. The green dash-dotted lines are true values of the parameters, which are time-varying. The red solid lines are estimated values by using the proposed robust algorithm, i.e., the weighted least squares with PS. The black dotted lines are estimated values without the robust algorithm, i.e., the conventional weighted least squares. Results show that the proposed robust algorithm is able to mitigate the negative impacts caused by outliers. Small MAPEs of the first scenario in Table I show that the proposed algorithm has good performance. For the second scenario in

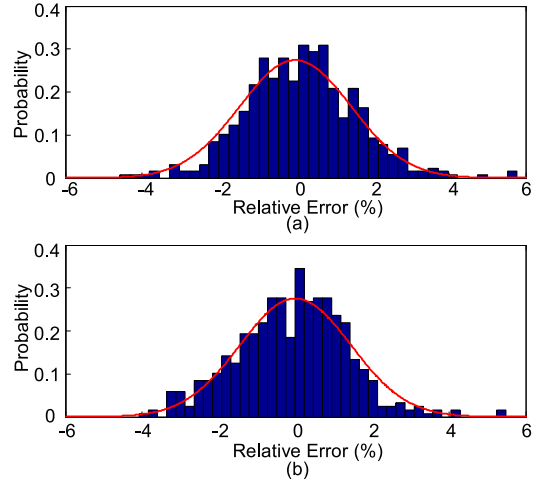


Fig. 8. (a) Relative errors of estimated active power. (b) Relative errors of estimated reactive power.

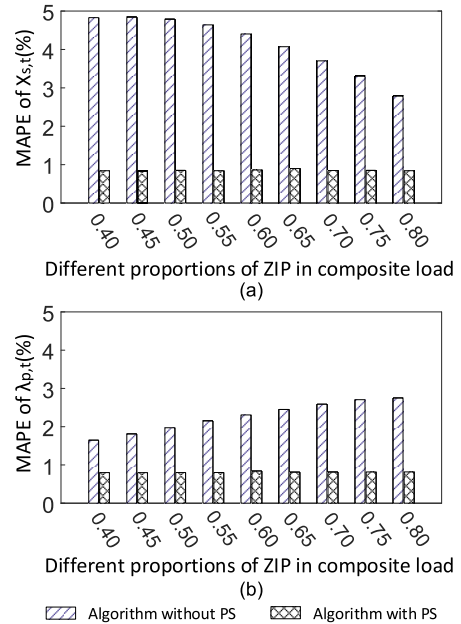
Fig. 9. (a) MAPEs of $X_{s,t}$ by using algorithm with PS and without PS. (b) MAPEs of $\lambda_{p,t}$ by using algorithm with PS and without PS.

Table I, the mean values of the parameters $\lambda_{p,t}$ and $\lambda_{q,t}$ are 0.4 and 0.4, respectively. The mean values of the other parameters are the same with those in the first scenario. Small MAPEs show that the proposed algorithm has good performance again.

Fig. 6 shows the estimated/true active power, and Fig. 7 shows the estimated/true reactive power. Fig. 8 (a) shows the probability density function of the relative errors of the estimated active power, and Fig. 8 (b) shows the probability density function of the relative errors of the estimated reactive power. The relative error is defined as (33), in which RE_t is the relative error at t , $v_{T,t}$ is the true value at t , and $v_{E,t}$ is the estimated value at t . The relative errors of estimated active power satisfy a Gaussian distribution with mean zero and standard deviation 1.4541, and the relative errors of estimated reactive power satisfy a Gaussian distribution with

TABLE I
MEAN ABSOLUTE PERCENTAGE ERROR (MAPE) (%)

		MAPE										
		$X_{s,t}$	$R_{s,t}$	$X_{r,t}$	$R_{r,t}$	$X_{m,t}$	$a_{p,t}$	$b_{p,t}$	$a_{q,t}$	$b_{q,t}$	$\lambda_{p,t}$	$\lambda_{q,t}$
1st Scenario	Algorithm with PS approach	0.817	0.874	0.824	0.779	0.987	0.875	0.864	0.798	0.796	0.789	0.884
	Algorithm without PS approach	2.911	1.097	2.744	0.892	1.031	1.901	1.408	0.825	0.801	2.883	1.748
2nd Scenario	Algorithm with PS approach	0.787	0.797	0.801	0.803	0.962	0.777	0.765	0.761	0.751	0.825	0.788
	Algorithm without PS approach	5.081	1.034	4.789	0.984	0.988	0.782	0.769	0.771	0.761	1.705	1.654

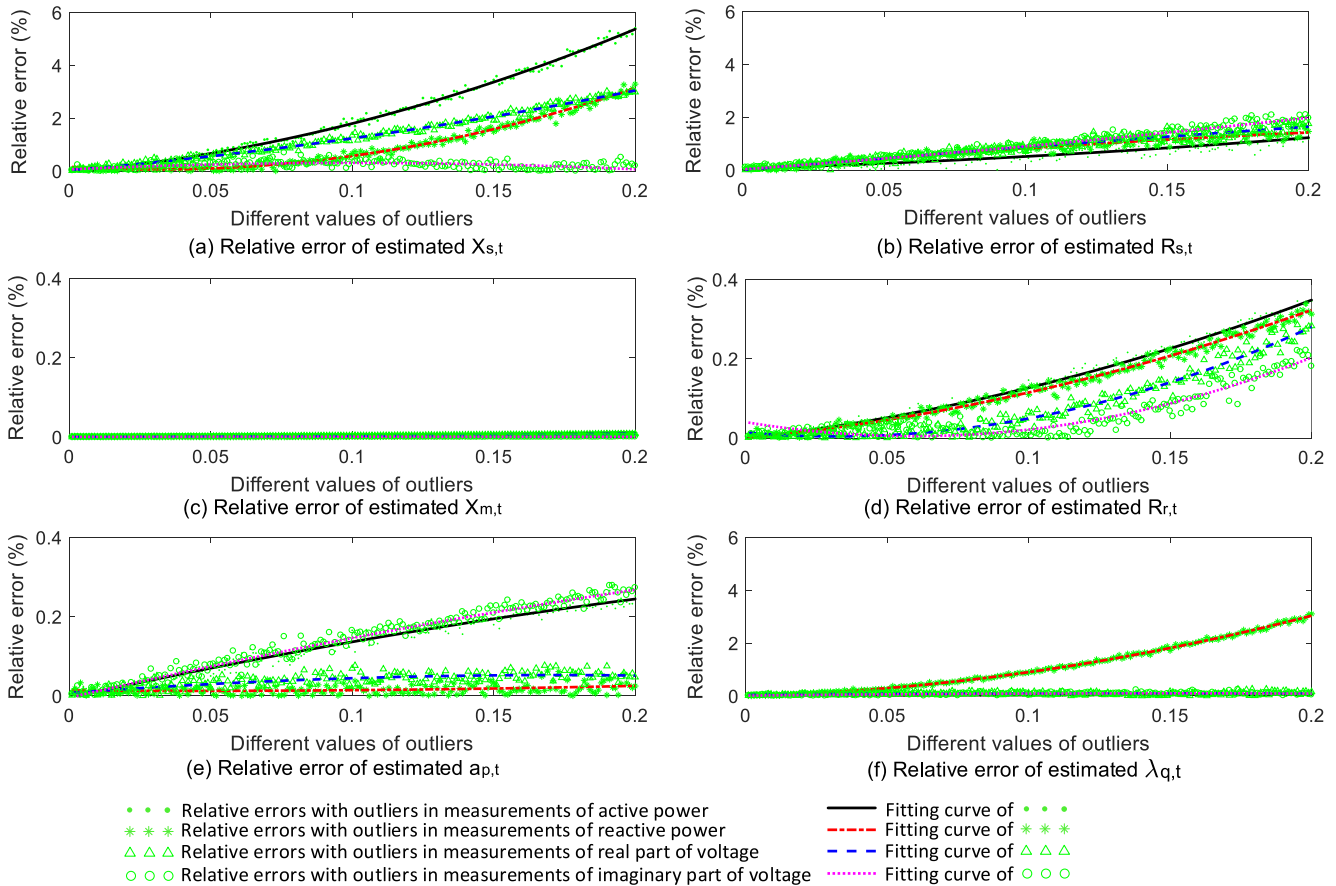


Fig. 10. Relative errors of estimated parameters to outliers in different measurements.

mean zero and standard deviation 1.4478. The small relative errors show the accuracy of the proposed method. RE_t and MAPE are defined as follows.

$$RE_t = |v_{T,t} - v_{E,t}| / |v_{m,t}| \times 100\% \quad (33)$$

$$MAPE = \left(\sum_t RE_t \right) / N \quad (34)$$

Fig. 9 shows MAPEs of the estimated $X_{s,t}$ and $\lambda_{p,t}$ with different proportions of ZIP in the composite load. The x-axis represents the proportion of ZIP in the composite load, and the y-axis represents MAPE. When the proportion of ZIP in the composite load has different values, MAPEs of the parameters identified by using the algorithm with PS have smaller values than those identified by using the algorithm without PS. In addition, MAPEs of the parameters identified by using the

algorithm with PS have small changes with different proportions of ZIP in the composite load. This means that MAPEs by using the algorithm with PS have the low sensitivity to different proportions of ZIP in the composite load.

2) *Sensitivity Analysis*: This section shows the sensitivity of different parameters to outliers. Fig. 10 shows the relative errors of the parameters to different values and different types of outliers. For example, the relative errors of the estimated $X_{s,t}$ increase with larger outliers of active power, reactive power and real part of voltage. But, the relative errors of the estimated $X_{s,t}$ have no obvious changes with larger outliers of imaginary part of voltage. For the estimated $R_{s,t}$, the relative errors with larger outliers of active power, reactive power, real part of voltage and imaginary part of voltage have the similar increase pattern. For the parameter $X_{m,t}$, outliers of active power, reactive power, real part of voltage and

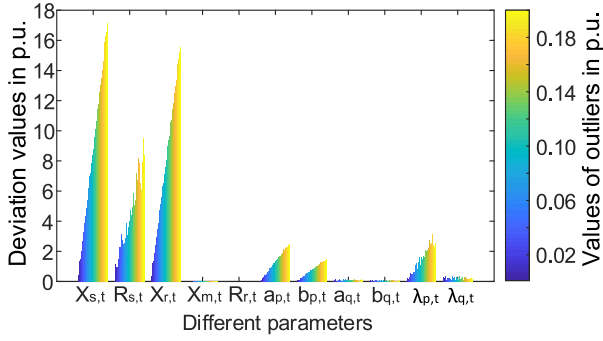


Fig. 11. Value of the first order partial derivative of the objective when active power outliers occur.

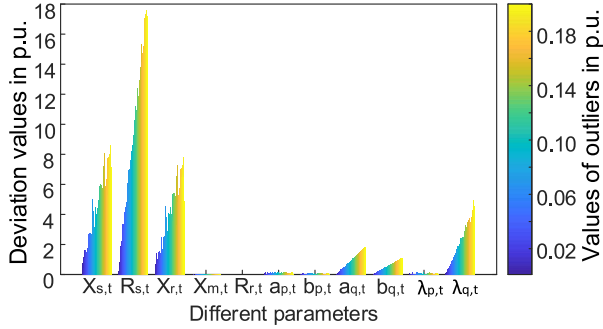


Fig. 12. Value of the first order partial derivative of the objective when reactive power outliers occur.

TABLE II
EIGENVALUES CORRESPONDING TO PARAMETERS

Parameters	$R_{s,t}$	$X_{s,t}$	$X_{m,t}$	$X_{r,t}$	$R_{r,t}$	H_t
Eigvalues (10^{-3})	0.798	1.392	1.635	1.712	1.724	2.243
Parameters	$a_{p,t}$	$b_{p,t}$	$a_{q,t}$	$b_{q,t}$	$\lambda_{p,t}$	$\lambda_{q,t}$
Eigvalues (10^{-3})	2.197	1.977	1.974	1.959	1.783	1.781

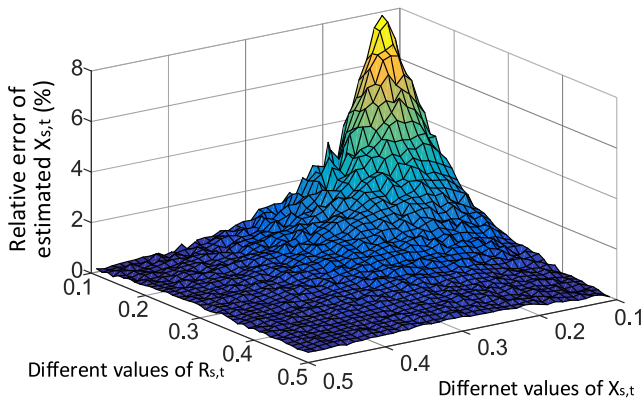


Fig. 13. Relative errors of estimated parameters $X_{s,t}$ with different $R_{s,t}$ and $X_{s,t}$.

imaginary part of voltage have small impacts on the relative errors.

According to Section IV-D, the amount of estimation updates can be qualitatively analyzed by using the first order

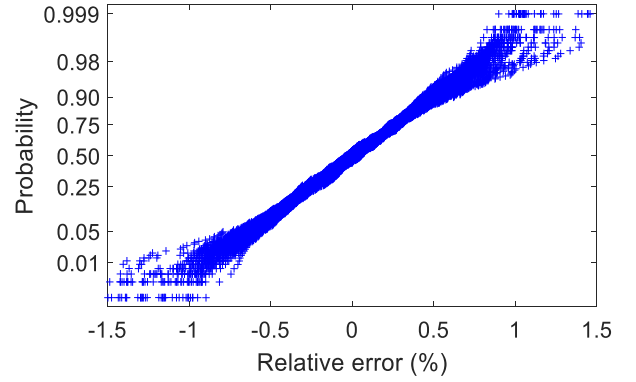


Fig. 14. Probability of relative errors of estimated active power of the composite ZIP and IM loads at different buses in IEEE 118-bus system.

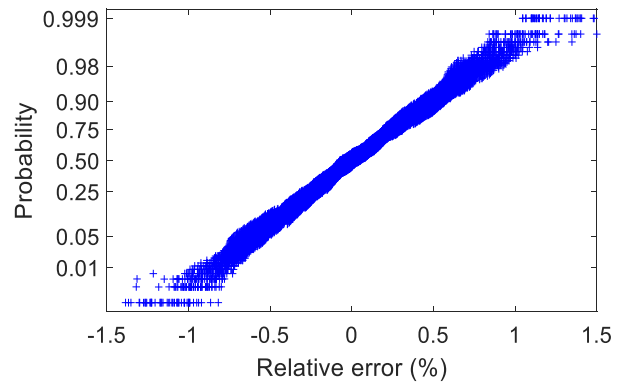


Fig. 15. Probability of relative errors of estimated reactive power of the composite ZIP and IM loads at different buses in IEEE 118-bus system.

partial derivative of the objective (F) and the eigenvalues of the inverse Hessian matrix. Table II shows the average eigenvalues corresponding to the parameters. Fig. 11 shows the first order partial derivative of the objective when there are outliers in measurements of active power. The x-axis represents the parameter, and the y-axis represents the value of the first order partial derivative. If the value of the first order partial derivative significantly increases with the increasing outliers, the relative errors of the estimated parameter tend to be sensitive to these outliers. For example, the first order partial derivative with respect to $X_{s,t}$ in Fig. 11 increases rapidly with the increasing outliers in measurements of active power, so the relative errors of the estimated $X_{s,t}$ markedly increase when outliers in measurements of active power increase, i.e., the black line in Fig. 10 (a). Since the eigenvalue corresponding to $X_{s,t}$ is larger than that corresponding to $R_{s,t}$ and the increment of the first order partial derivative with respect to $X_{s,t}$ is larger than that with respect to $R_{s,t}$, the relative errors of the estimated $X_{s,t}$ are also larger than that of the estimated $R_{s,t}$, i.e., the black lines in Fig. 10 (a) and (b). This indicates that $X_{s,t}$ is more sensitive to the outliers in measurements of active power compared to $R_{s,t}$. Because the first order partial derivative with respect to $X_{m,t}$ is very small with the increasing outliers in measurements of active power, as shown in Fig. 11, the relative errors of the estimated $X_{m,t}$ are also small,

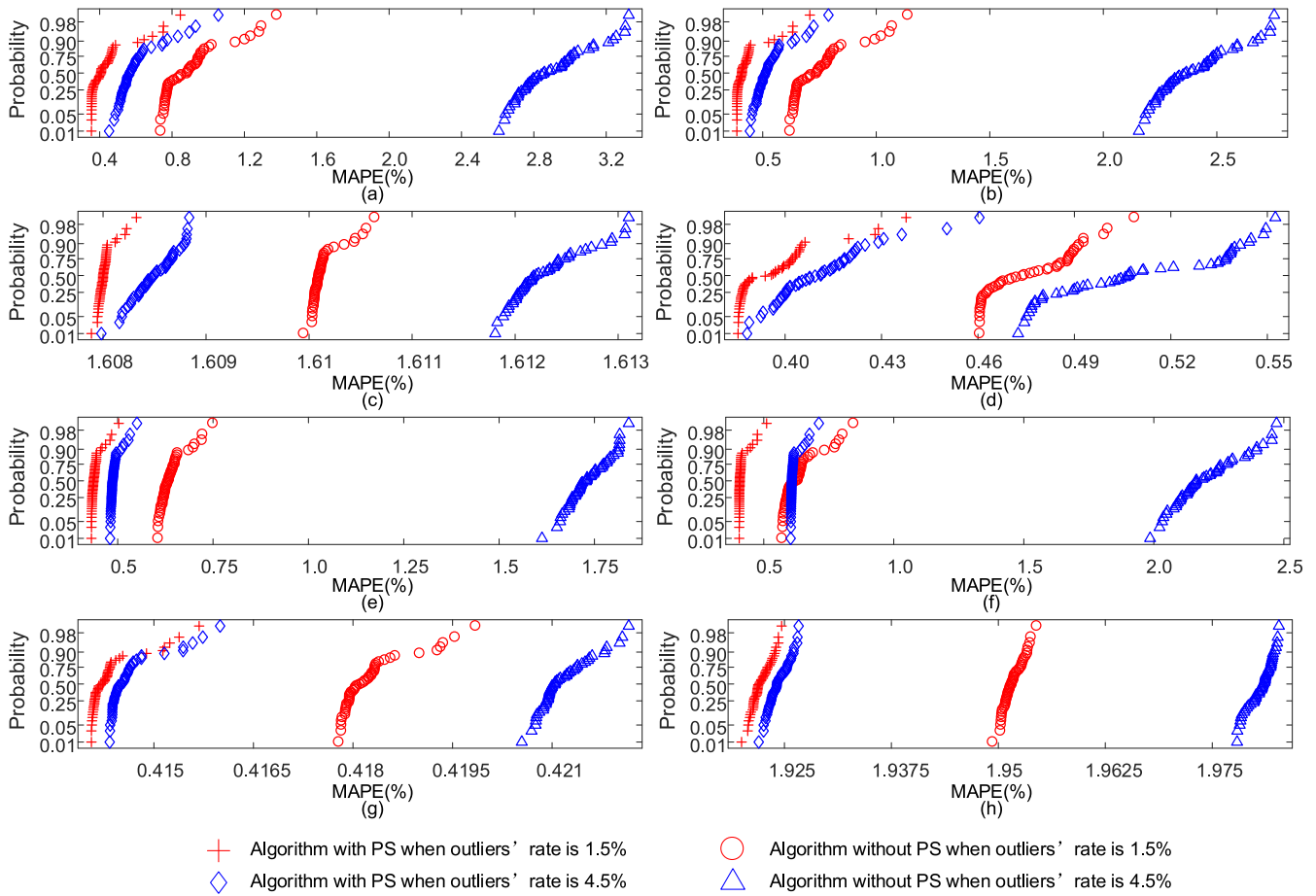


Fig. 16. MAPEs of $X_{s,t}$ (a), $X_{r,t}$ (b), $X_{m,t}$ (c), $R_{s,t}$ (d), $\lambda_{q,t}$ (e), $\lambda_{p,t}$ (f), $b_{q,t}$ (g), and $a_{q,t}$ (h).

as shown in Fig. 10 (c). This indicates that $X_{m,t}$ is not sensitive to outliers in measurements of active power. Similarly, the sensitivities of other parameters to outliers in measurements of active power can be qualitatively analyzed.

Fig. 12 shows the first order partial derivative of the objective when there are outliers in measurements of reactive power. If the value of the first order partial derivative significantly increases with increasing values of the outliers, the relative errors of the estimated parameter tend to be sensitive to these outliers. For example, the first order partial derivative with respect to $X_{s,t}$ has a large value with a large outlier, so the relative errors of estimated $X_{s,t}$ remarkably increase with large outliers in measurements of reactive power. Furthermore, since the increment with respect to $X_{s,t}$ in Fig. 12 is smaller than that in Fig. 11, the relative errors with reactive power outliers are smaller than those with active power outliers, i.e., the values of the red dash-dotted are smaller than those of the black solid line in Fig. 10 (a). This indicates that the sensitivity of $X_{s,t}$ to outliers in measurements of active power is higher compared to outliers in measurements of reactive power. Similarly, the sensitivities of other parameters to outliers in measurements of reactive power can be qualitatively analyzed.

In addition, Fig. 13 shows the relative errors of the estimated $X_{s,t}$ with active power outliers when $X_{s,t}$ and $R_{s,t}$ have different values. The x-axis and the y-axis represent $R_{s,t}$ and

$X_{s,t}$, respectively. The z-axis represents the relative error of the estimated $X_{s,t}$. When the values of $R_{s,t}$ and $X_{s,t}$ are both 0.1, the relative error of the estimated $X_{s,t}$ is around 8%. When the values of $R_{s,t}$ and $X_{s,t}$ are both 0.5, the relative error of the estimated X_s is around 0.2%. Results show that the accuracy of the estimated parameters is impacted by the values of parameters.

C. IEEE 118-Bus System

This section shows the results on the IEEE 118-bus system in which 50 buses are connected to composite ZIP and IM loads. For each composite ZIP and IM load, there are 500 samples for simulation, and the sample time is 0.1s. Table III shows the buses with composite ZIP and IM loads. The mean values of the parameters $R_{s,t}$, $X_{s,t}$, $X_{m,t}$, $X_{r,t}$, $R_{r,t}$, H_t , $a_{p,t}$, $b_{p,t}$, $a_{q,t}$, $b_{q,t}$, $\lambda_{p,t}$, $\lambda_{q,t}$ for each composite ZIP and IM model are 0.07, 0.5, 4, 0.4, 0.01, 20, 0.3, 0.5, 0.2, 0.4, 0.4 and 0.4. A Gaussian random variable with zero mean and standard deviation MVP/100 is added to each parameter to simulate continuous parameter changes. Each measurement is assumed to have a Gaussian noise with zero mean and standard deviation of 0.005.

Fig. 14 shows the probabilities of the relative errors of the estimated active power of the composite loads at different buses and samples. The x-axis presents the relative error, and

TABLE III
BUSES WITH COMPOSITE ZIP AND IM LOADS

Buses with composite ZIP and IM loads
2, 3, 5, 7, 9, 11, 13, 16, 17, 20, 21, 22, 23, 28, 29
30, 33, 35, 37, 38, 39, 41, 43, 44, 45, 47, 48, 50, 51, 52
53, 57, 58, 60, 63, 64, 67, 68, 71, 75, 78, 79, 81, 82, 83
84, 86, 88, 93, 94

the y-axis presents the probability. Results show that the range of the most relative errors of the estimated active power is from -1.5% to 1.5% . Fig. 15 shows the probabilities of the relative errors of the estimated reactive power of the composite loads. Results show that the range of the most relative errors of the estimated reactive power is from -1.5% to 1.5% . The small relative errors validate the effectiveness of the proposed parameter identification technique.

MAPEs of the parameters $X_{s,t}$, $X_{r,t}$, $X_{m,t}$, $R_{s,t}$, $\lambda_{q,t}$, $\lambda_{p,t}$, $b_{q,t}$ and $a_{q,t}$ are presented in Figs. 16 (a), (b), (c), (d), (e), (f), (g), and (h), respectively. The x-axis for each figure represents MAPE, and the y-axis represents the probability. The results with different outliers' rates and different algorithms are compared. The red markers '+' are results by using the algorithm with PS when the outliers' rate is 1.5% , and the red markers 'o' are results by using the algorithm without PS when the outliers' rate is 1.5% . The blue markers '◇' are results by using the algorithm with PS when the outliers' rate is 4.5% , and the blue markers '△' are results by using the algorithm without PS when the outliers' rate is 4.5% . With the same outliers' rate, MAPEs of the estimated parameters by using the algorithm with PS are smaller than those without PS. For example, when the outliers' rate is 1.5% , MAPEs of $X_{s,t}$ by using the algorithm with PS (the red markers '+' in Fig. 16 (a)) is smaller than those without PS (the red markers 'o' in Fig. 16 (a)). In addition, with the same approach, MAPEs of the estimated parameters with a lower outliers' rate are smaller than those with a higher outliers' rate. For example, MAPEs of $X_{s,t}$ by using the algorithm with PS when the outliers' rate is 1.5% (the red markers '+' in Fig. 16 (a)) are smaller than those with the 4.5% outliers' rate (the blue markers '◇' in Fig. 16 (a)). Small MAPEs show that the proposed algorithm has good performance.

VI. CONCLUSION

This paper proposed a robust time-varying parameter identification technique for the composite ZIP and IM load model. The data redundancy for parameter identification was guaranteed by using the batch-model regression. Down-weighting coefficients of measurements, used to deal with outliers, were achieved by calculating robust distances of a k -time sequence with the PS approach. The optimization of the weighted squares error was solved by the Newton-Raphson approach with the estimated parameters at the previous sample time as an initial iteration value. Sensitivity analysis was conducted to qualitatively achieve the change patterns of the parameters

to different types of outliers. The major findings are as follows. 1) The proposed method can identify the time-varying parameters of the composite ZIP and IM model with a high accuracy. 2) The down-weighting coefficients based on the PS approach can robustly deal with outliers in measurements. 3) The first order partial derivative of the objective can be used to qualitatively analyze the sensitivity of the parameters to outliers.

The wide deployment of renewable energy sources introduces additional dynamics into power systems as inverter-based distributed generators (DGs) are now interfaced with the systems. This is especially true for a microgrid that is a cluster of loads and DGs. In the future work, we will consider the influences of these inverter-based DGs on the dynamic load modeling.

REFERENCES

- [1] S. R. Bull, "Renewable energy today and tomorrow," *Proc. IEEE*, vol. 89, no. 8, pp. 1216–1226, Aug. 2001.
- [2] B. Kroposki *et al.*, "Achieving a 100% renewable grid: Operating electric power systems with extremely high levels of variable renewable energy," *IEEE Power Energy Mag.*, vol. 15, no. 2, pp. 61–73, Mar./Apr. 2017.
- [3] C. C. Chan and Y. S. Wong, "Electric vehicles charge forward," *IEEE Power Energy Mag.*, vol. 2, no. 6, pp. 24–33, Nov./Dec. 2004.
- [4] Z. Wang and J. Wang, "Time-varying stochastic assessment of conservation voltage reduction based on load modeling," *IEEE Trans. Power Syst.*, vol. 29, no. 5, pp. 2321–2328, Sep. 2014.
- [5] J. Zhao, Z. Wang, C. Chen, and G. Zhang, "Robust voltage instability predictor," *IEEE Trans. Power Syst.*, vol. 32, no. 2, pp. 1578–1579, Mar. 2017.
- [6] C. Wang, Y. Hou, F. Qiu, S. Lei, and K. Liu, "Resilience enhancement with sequentially proactive operation strategies," *IEEE Trans. Power Syst.*, vol. 32, no. 4, pp. 2847–2857, Jul. 2017.
- [7] G. Giorgi and C. Narduzzi, "Performance analysis of Kalman-filter-based clock synchronization in IEEE 1588 networks," *IEEE Trans. Instrum. Meas.*, vol. 60, no. 8, pp. 2902–2909, Aug. 2011.
- [8] A. Arif *et al.*, "Load modeling—A review," *IEEE Trans. Smart Grid*, to be published.
- [9] I. Dzafic, M. Glavic, and S. Tesnjak, "A component-based power system model-driven architecture," *IEEE Trans. Power Syst.*, vol. 19, no. 4, pp. 2109–2110, Nov. 2004.
- [10] D. Kosterev *et al.*, "Load modeling in power system studies: WECC progress update," in *Proc. IEEE PES Gen. Meeting*, Pittsburgh, PA, USA, Jul. 2008, pp. 1–8.
- [11] H. Renmu, M. Jin, and D. J. Hill, "Composite load modeling via measurement approach," *IEEE Trans. Power Syst.*, vol. 21, no. 2, pp. 663–672, May 2006.
- [12] J. Ma, D. Han, R.-M. He, Z.-Y. Dong, and D. J. Hill, "Reducing identified parameters of measurement-based composite load model," *IEEE Trans. Power Syst.*, vol. 23, no. 1, pp. 76–83, Feb. 2008.
- [13] C. Wang, Z. Qin, Y. Hou, and J. Yan, "Multi-area dynamic state estimation with PMU measurements by an equality constrained extended Kalman filter," *IEEE Trans. Smart Grid*, to be published.
- [14] I. F. Visconti, D. A. Lima, J. M. C. D. S. Costa, and N. R. D. B. C. Sobrinho, "Measurement-based load modeling using transfer functions for dynamic simulations," *IEEE Trans. Power Syst.*, vol. 29, no. 1, pp. 111–120, Jan. 2014.
- [15] D. Han, J. Ma, R.-M. He, and Z.-Y. Dong, "A real application of measurement-based load modeling in large-scale power grids and its validation," *IEEE Trans. Power Syst.*, vol. 24, no. 4, pp. 1756–1764, Nov. 2009.
- [16] P. Kundur, *Power System Stability and Control*. New York, NY, USA: McGraw-Hill, 1994.
- [17] K.-H. Tseng, W.-S. Kao, and J.-R. Lin, "Load model effects on distance relay settings," *IEEE Trans. Power Del.*, vol. 18, no. 4, pp. 1140–1146, Oct. 2003.

- [18] IEEE Task Force on Load Representation for Dynamic Performance, "Standard load models for power flow and dynamic performance simulation," *IEEE Trans. Power Syst.*, vol. 10, no. 3, pp. 1302–1313, Aug. 1995.
- [19] W. Price, K. Wirgau, A. Murdoch, and F. Nozari, "Load modeling for power flow and transient stability studies," EPRI, Palo Alto, CA, USA, Tech. Rep. EL-5003, 1987.
- [20] "Extended transient-midterm stability program," EPRI, Palo Alto, CA, USA, Tech. Rep. EPRI-TR-102004, 1993.
- [21] D. J. Hill, "Nonlinear dynamic load models with recovery for voltage stability studies," *IEEE Trans. Power Syst.*, vol. 8, no. 1, pp. 166–176, Feb. 1993.
- [22] W. Xu and Y. Mansour, "Voltage stability analysis using generic dynamic load models," *IEEE Trans. Power Syst.*, vol. 9, no. 1, pp. 479–493, Feb. 1994.
- [23] Y. Ge *et al.*, "An event-oriented method for online load modeling based on synchrophasor data," *IEEE Trans. Smart Grid*, vol. 6, no. 4, pp. 2060–2068, Jul. 2015.
- [24] W.-S. Kao, C.-J. Lin, C.-T. Huang, Y.-T. Chen, and C.-Y. Chiou, "Comparison of simulated power system dynamics applying various load models with actual recorded data," *IEEE Trans. Power Syst.*, vol. 9, no. 1, pp. 248–254, Feb. 1994.
- [25] J. V. Milanovic, K. Yamashita, S. M. Villanueva, S. Ž. Djokic, and L. M. Korunović, "International industry practice on power system load modeling," *IEEE Trans. Power Syst.*, vol. 28, no. 3, pp. 3038–3046, Aug. 2013.
- [26] IEEE Task Force on Load Representation for Dynamic Performance, "Load representation for dynamic performance analysis (of power systems)," *IEEE Trans. Power Syst.*, vol. 8, no. 2, pp. 472–482, May 1993.
- [27] I. A. Hiskens, "Nonlinear dynamic model evaluation from disturbance measurements," *IEEE Trans. Power Syst.*, vol. 16, no. 4, pp. 702–710, Nov. 2001.
- [28] Q. Liu, Y. Chen, and D. Duan, "The load modeling and parameters identification for voltage stability analysis," in *Proc. Int. Conf. Power Syst. Technol.*, vol. 4, Kunming, China, 2002, pp. 2030–2033.
- [29] J. Zhao, M. Netto, and L. Mili, "A robust iterated extended Kalman filter for power system dynamic state estimation," *IEEE Trans. Power Syst.*, vol. 32, no. 4, pp. 3205–3216, Jul. 2017.
- [30] J. A. de Kock, F. S. van der Merwe, and H. J. Vermeulen, "Induction motor parameter estimation through an output error technique," *IEEE Trans. Energy Convers.*, vol. 9, no. 1, pp. 69–76, Mar. 1994.
- [31] P. Ju, E. Handschin, and D. Karlsson, "Nonlinear dynamic load modelling: Model and parameter estimation," *IEEE Trans. Power Syst.*, vol. 11, no. 4, pp. 1689–1697, Nov. 1996.
- [32] T. Hiyama, M. Tokieda, W. Hubbi, and H. Andou, "Artificial neural network based dynamic load modeling," *IEEE Trans. Power Syst.*, vol. 12, no. 4, pp. 1576–1583, Nov. 1997.
- [33] V. Knyazkin, C. A. Canizares, and L. H. Soder, "On the parameter estimation and modeling of aggregate power system loads," *IEEE Trans. Power Syst.*, vol. 19, no. 2, pp. 1023–1031, May 2004.
- [34] A. Miranian and K. Rouzbehi, "Nonlinear power system load identification using local model networks," *IEEE Trans. Power Syst.*, vol. 28, no. 3, pp. 2872–2881, Aug. 2013.
- [35] K. G. Boroojeni *et al.*, "A novel multi-time-scale modeling for electric power demand forecasting: From short-term to medium-term horizon," *Elect. Power Syst. Res.*, vol. 142, pp. 58–73, Jan. 2017.
- [36] J. Zhao, Z. Wang, and J. Wang, "Robust time-varying load modeling for conservation voltage reduction assessment," *IEEE Trans. Smart Grid*, to be published.
- [37] N. Watson and J. Arrillaga, *Power Systems Electromagnetic Transients Simulation*. London, U.K.: Inst. Elect. Eng., 2003.
- [38] D. Donoho, "Breakdown properties of multivariate location estimators," Ph.D. dissertation, Dept. Stat., Harvard Univ., Cambridge, MA, USA, 1982. [Online]. Available: <https://statweb.stanford.edu/donoho/Reports/Oldies/BPMLE.pdf>
- [39] D. L. Donoho and M. Gasko, "Breakdown properties of location estimates based on halfspace depth and projected outlyingness," *Ann. Stat.*, vol. 20, no. 4, pp. 1803–1827, Dec. 1992.
- [40] M. A. Gandhi and L. Mili, "Robust Kalman filter based on a generalized maximum-likelihood-type estimator," *IEEE Trans. Signal Process.*, vol. 58, no. 5, pp. 2509–2520, May 2010.



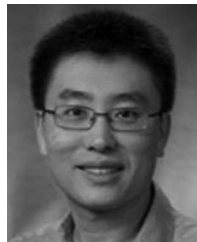
Chong Wang (M'16) received the B.E. and M.S. degrees in electrical engineering from Hohai University, Nanjing, China, in 2009 and 2012, respectively, and the Ph.D. degree in electrical engineering from the University of Hong Kong, Hong Kong, in 2016. He was a Post-Doctoral Researcher with the University of Hong Kong in 2016, and is currently a Post-Doctoral Researcher with Iowa State University.

His research interests include optimization and its applications in power systems, smart grids, integration of renewable energy sources, and cyber-physical systems.



Zhaoyu Wang (S'13–M'15) received the B.S. and M.S. degrees in electrical engineering from Shanghai Jiaotong University in 2009 and 2012, respectively, and the M.S. and Ph.D. degrees in electrical and computer engineering from the Georgia Institute of Technology in 2012 and 2015, respectively. He is the Harpole Pentair Endowed Assistant Professor with Iowa State University. He was a Research Aid with Argonne National Laboratory in 2013, and an Electrical Engineer with Corning Inc. in 2014. His research interests include power distribution systems, microgrids, renewable integration, power system resiliency, demand response, and voltage/VAR control. He was a recipient of the IEEE PES General Meeting Best Paper Award in 2017 and the IEEE Industrial Application Society Prize Paper Award in 2016. He is an Editor of the IEEE TRANSACTIONS ON SMART GRID and the IEEE PES LETTERS. He is the Secretary of IEEE Power and Energy Society (PES) Award Subcommittee. His research projects are currently funded by the National Science Foundation, the Department of Energy, National Laboratories, PSERC, Iowa Energy Center, and industry.

His research projects are currently funded by the National Science Foundation, the Department of Energy, National Laboratories, PSERC, Iowa Energy Center, and industry.



Jianhui Wang (M'07–SM'12) received the Ph.D. degree in electrical engineering from the Illinois Institute of Technology, Chicago, IL, USA, in 2007. He is currently an Associate Professor with the Department of Electrical Engineering, Southern Methodist University, Dallas, TX, USA. He also holds a joint appointment as a Section Lead for Advanced Power Grid Modeling with the Energy Systems Division, Argonne National Laboratory, Argonne, IL, USA. He was a recipient of the IEEE PES Power System Operation Committee Prize

Paper Award in 2015. He is the Secretary of the IEEE Power and Energy Society (PES) Power System Operations, Planning and Economics Committee. He is an Associate Editor of the *Journal of Energy Engineering* and an Editorial Board Member of *Applied Energy*. He has held visiting positions in Europe, Australia, and Hong Kong including a VELUX Visiting Professorship with the Technical University of Denmark. He is the Editor-in-Chief of the IEEE TRANSACTIONS ON SMART GRID and an IEEE PES Distinguished Lecturer.



Dongbo Zhao (S'10–M'14–SM'16) received the B.S. degree from Tsinghua University, China, the M.S. degree from Texas A&M University, College Station, TX, USA, and the Ph.D. degree from the Georgia Institute of Technology, Atlanta, GA, USA, all in electrical engineering. He was an Research and Development Engineer with Eaton Corporation from 2014 to 2016, and with ABB from 2010 to 2011. He is currently an Energy System Scientist with Argonne National Laboratory, Lemont, IL, USA. His research interests include

power system control, protection, reliability analysis, transmission and distribution automation, and electric market optimization. He is a member of IEEE PES Society, Smart Grid Community, and IEEE Young Professionals. He is an Associate Editor of the *IET Renewable Power Generation*, an Editor of *International Transactions on Electrical Energy Systems*, and an Associate Editor of IEEE ACCESS.